UDC 551.511.33:551.558.1

Laboratory Simulation of Wake Effects on Second and Third Thermals in a Series

EUGENE M. WILKINS[1], **YOSHIKAZU SASAKI, and ERNEST W. MARION**[2]
University of Oklahoma, Norman, Okla.

ABSTRACT—Individual thermals rising through the atmosphere may encounter the wake of one or more thermals that started their rise at an earlier time. Laboratory simulations show that the growth rate of second and third thermals in a series is enhanced relative to that of a solitary thermal. The enhancement is due to a gain in momentum from the wake of a preceding thermal, and equations are developed for predicting the amount of enhancement as a function of the delay time between thermals. Agreement with experimental data is good for first and second thermals. The third thermal was found to have a growth rate very similar to that of a second thermal. Theory agrees to the extent that only a slight increase is predicted, and this amount could have been lost within the experimental error. Thus, it appears that by the time the third thermal in a series occurs, an equilibrium condition has been reached as far as the thermal growth rate and velocity field are concerned.

1. INTRODUCTION

Free convection is convective motion that is due entirely to buoyancy forces that arise from variations in temperature or density. In the atmosphere, for example, free convection occurs when an air parcel has a temperature slightly warmer than its environment and rises because of its buoyancy. Cumulus-type clouds that are formed by free convection are often referred to as thermals. Elements of free convection have been simulated in the laboratory by the release of a buoyant element to form a solitary thermal in a neutral environment. The solitary thermal has been studied in great detail in an effort to understand convection in the atmosphere. The probable occurrence of successive convective elements originating from the same point due to terrain irregularities, for example, has stimulated an interest in the investigation of the effect of the wake of a preceding thermal on a following thermal. The purpose of this work is to investigate the wake effects on second and third thermals in a series. We will utilize results obtained by previous investigators of solitary thermals.

In the study of free convection, thermals from instantaneous point sources and plumes from maintained point sources have been investigated extensively. Batchelor (1954) investigated free convection in fluids and showed how experiments of this type were related to atmospheric convection by describing the common ground between them. He used dimensional analysis and similarity arguments in his treatment of plumes and thermals for both laminar and turbulent flow. Morton et al. (1956) developed two separate sets of equations to describe the conservation of volume, momentum, and buoyancy for the plume and thermal. Variables of the plume were given as a function of height and for the thermal as a function of time. The conservation equations of Morton et al. (1956), modified to include wake effects, form the basic theory for the solitary thermal used in this work. The modification for the second and third thermals presented in this paper is based on the assumption that the wake velocity decays according to the same law as the cap velocity.

Scorer (1957) conducted experiments to determine the proportionality constants that arise from dimensional analysis. The experimental technique used was to inject a small amount of cloud material, a negatively buoyant dyed fluid, into a tank of water and to record the growth photographically. Woodward (1959) used the same experimental technique, along with tracer particles, to determine the circulation in a thermal. Streak photographs showed that the vertical velocity at the center of the thermal was twice as great as at the top; and the downward velocity at the edge was about half as great as the vertical velocity of the top (thermal cap). A visible circulation pattern was observed that is a result of cloud elements moving upward in the center and downward at the periphery of the thermal. This resembles a ring or toroidal-type vortex.

The effect of a rotation field on a thermal, although not considered in this work, has been investigated. Wilkins et al. (1969) modified the conservation equations of Morton et al. (1956) to include the effect of a rotation field on a thermal. The rotation was shown to suppress the growth of the thermal, and this effect was verified experimentally.

Wake effects on second thermals in a series were investigated both experimentally and theoretically by Wilkins et al. (1971*a*, 1971*b*), who modified the momentum conservation equation of Morton et al. (1956) to state the conservation of relative momentum of a wake-imbedded

[1] Also at Advanced Technology Center, Inc., Dallas, Tex.
[2] Now affiliated with the National Severe Storms Laboratory, National Oceanic and Atmospheric Administration, Norman, Okla.

second thermal. Schauss (1970) developed analytic solutions for the second thermal through the assumption of an exponential decay of the wake velocity. Wilkins et al. (1971*a*) also modified the momentum conservation equation to include the interaction of forces due to buoyancy and rotation-suppression. They developed analytical solutions for the second thermal by assuming that the wake velocity is proportional to the vertical velocity of the preceding thermal and the magnitude of the effect is dependent on the amount of the wake intercepted by the second thermal (increasing with growth). The vertical velocity for both the first thermal and its wake was assumed to decay according to the same law (inverse square root of time).

The theoretical development of wake effects on second and third thermals in a series, presented in this paper, is based on the same modified conservation equations except that the assumption concerning the effect on the thermal of intercepting only a portion of the wake is dropped. The dropped assumption seemed rather artificial. It made the problem tractable, but the solutions obtained do not fit the new experimental data nearly as well as the numerical solutions given in this paper. The wake velocity encountered by a thermal will simply be assumed to equal the vertical velocity of the preceding thermal, corrected for the time delay between thermals. The momentum equation will also be generalized for the nth thermal in a series.

The time interval between the successive thermals is of basic importance in the investigation of wake effects on succeeding thermals. A "short" time delay will result in a second thermal rapidly overtaking the preceding thermal. A "long" time delay can be described as one that allows the wake velocity to decay to the point where it has little or no effect on succeeding thermals. An "intermediate" time delay results in an increased vertical velocity of the second thermal but does not necessarily result in overtaking. Overtaking, if it occurs, is a problem in this investigation of wake effects because the second thermal is no longer entirely in the wake of a preceding thermal. This would invalidate one of our assumptions. This investigation is limited to the consideration of wake effects and, for this reason, an intermediate time delay was selected to assure that overtaking did not occur in the experiments.

Wilkins et al. (1971*a*) encountered an experimental difficulty that hampered the investigation of second thermals in a series. The difficulty was that, after a short period of time, the second thermal began to be obscured by cloud elements trailing behind the preceding one. This made it difficult to distinguish the boundaries of the second thermal. This, coupled with the fact that the lifetime of their second thermals was only about 5s, limited the opportunity to study the growth of the second thermal. The experimental technique for the present investigation is to use a thermal with a longer lifetime and to provide an unobstructed view of the thermal under investigation. The lifetime of the thermal is increased by using a small quantity of low-buoyancy dyed fluid as cloud material in the simulation. An unobstructed view of the wake-affected thermal is provided by making the preceding thermal transparent (by simply omitting the dye).

TABLE 1.—*Symbols used in this paper*

E	entrainment rate
F	buoyancy force per unit mass
V	thermal volume
w	vertical velocity of thermal
b	sphere-equivalent radius of thermal
g	gravitational acceleration
h	height of the thermal
t	time
α	entrainment constant
ρ	density of buoyant element
ρ_0	density of environment
τ	time delay between thermal injections

2. GOVERNING EQUATIONS

The development of the governing equations for a second and third thermal in series involves modifying the basic conservation equations of Morton et al. (1956) for a solitary thermal to account for the momentum gained from a wake. The key assumptions of Morton et al. are: (1) entrainment is proportional to vertical velocity; (2) lateral profiles of the mean vertical velocity and mean buoyancy force are similar at all levels; and (3) local variations of density are small when compared with the reference density, which is defined here as the density of the environmental fluid. The same assumptions are made in the development to follow.

The symbols used in the development are given in table 1. Throughout the paper, subscripts of 1, 2, and 3 will be used to denote terms applying to first, second, and third thermals, respectively. The units of all terms will be in the cgs system.

The three basic conservation equations developed by Morton et al. (1956) are:

$$\text{volume } \frac{d}{dt}\left(\frac{4}{3}\pi b_1^3\right)=4\pi b_1^2\alpha_1 w_1, \tag{1}$$

$$\text{momentum } \frac{d}{dt}\left(\frac{4}{3}\pi b_1^3 w_1\right)=\frac{4}{3}\pi b_1^3\frac{\rho_0-\rho}{\rho_0}g=F, \tag{2}$$

and

$$\text{buoyancy force } \frac{d}{dt}\left(\frac{4}{3}\pi b_1^3\frac{\rho_0-\rho}{\rho_0}g\right)=\frac{dF}{dt}=0. \tag{3}$$

A set of solutions for the conservation eq (1)–(3) was given by Morton et al. (1956). These are given below with some change of notation:

$$b_1=\alpha_1 h_1=\left(\frac{3\alpha_1 F}{2\pi}\right)^{1/4}t^{1/2}, \tag{4}$$

$$w_1=\frac{1}{2\alpha_1}\left(\frac{3\alpha_1 F}{2\pi}\right)^{1/4}t^{-1/2}, \tag{5}$$

and

$$E_1=\frac{1}{V_1}\frac{dV_1}{dt}=\frac{3}{2}t^{-1}. \tag{6}$$

The boundary conditions are $b=0$ when $t=0$ and momentum$=0$ when $t=0$.

Second Thermal in Series

The equation for the vertical velocity, w_1, of a preceding thermal, corrected for lapsed time, is used to estimate a wake velocity in the development of the theory for the second thermal in a series. This procedure entails the assumption that the first thermal in a series will behave as a solitary thermal and will not be affected by the thermal following in its wake. Probably such an assumption is reasonable up to the time that the first thermal is overtaken by the second one. We also assume that the ambient density, ρ_0, is unaffected by the mixing of preceding thermals into the environment. This assumption is justified in the single-source convection discussed here but probably not in the case of multiple sources, as shown by Sasaki (1967).

Equation (2) is the only one of the set [eq (1)–(3)] developed by Morton et al. (1956) that is changed. The change, it will be seen, is to account for an increase in momentum of the second thermal that is gained from the wake velocity of the preceding thermal. In the case of the second thermal, the wake velocity at time t is assumed to be equal to the vertical velocity of the preceding thermal at time $t+\tau$ where τ is the time delay of the second thermal injection.

The conservation equations for the second thermal are:

$$\text{volume } \frac{d}{dt}\left(\frac{4}{3}\pi b_2^3\right)=4\pi b_2^2\alpha_2 w_2, \tag{7}$$

$$\text{momentum } \frac{d}{dt}\left(\frac{4}{3}\pi b_2^3 w_2\right)=F+\underline{\frac{d}{dt}\left(\frac{4}{3}\pi b_2^3 w_1\right)}, \tag{8}$$

and

$$\text{buoyancy force } \frac{d}{dt}\left(\frac{4}{3}\pi b_2^3\frac{\rho_0-\rho}{\rho_0}g\right)=\frac{dF}{dt}=0 \tag{9}$$

where

$$w_1=\frac{1}{2\alpha_1}\left(\frac{3\alpha_1 F}{2\pi}\right)^{1/4}(t+\tau)^{-1/2}. \tag{10}$$

The additional term in the momentum eq (8) has been underlined.

From the integration of the momentum eq (8) and the initial condition $b_2=0$ at $t=0$, we have

$$b_2^3 w_2=\frac{3Ft}{4\pi}+b_2^3 w_1. \tag{11}$$

From eq (7), the relation

$$w_2=\frac{1}{\alpha_2}\frac{db_2}{dt}, \tag{12}$$

when substituted into eq (11) along with the expression for w_1 from eq (10), gives

$$b_2^3\frac{db_2}{dt}=\frac{3\alpha_2 Ft}{4\pi}+b_2^3\frac{\alpha_2}{2\alpha_1}\left(\frac{3\alpha_1 F}{2\pi}\right)^{1/4}(t+\tau)^{-1/2}. \tag{13}$$

Equation (13) is nonlinear but is easily solved for b_2 by numerical methods. It is then possible to solve numerically for the other variables; that is, vertical velocity from eq (12), height from

$$h_2=\frac{b_2}{\alpha_2}, \tag{14}$$

and entrainment rate from

$$E_2=\frac{1}{V_2}\frac{dV_2}{dt}=\frac{3}{b_2}\frac{db_2}{dt}. \tag{15}$$

Equation (13) may be written in the form

$$y^3(y'-1)=x(x^2-1) \tag{16}$$

where the variables are nondimensionalized as

$$y=\frac{b_2}{\left(\frac{3\alpha F}{2\pi}\right)^{1/4}\tau^{1/2}} \tag{17}$$

and

$$x^2=\frac{t+\tau}{\tau}. \tag{18}$$

The prime denotes a derivative with respect to x. The assumption $\alpha=\alpha_1=\alpha_2$ has been made to obtain eq (16). This equation may be solved easily by numerical methods. The solution is valid for all values of τ, α, and F provided only that overtaking does not occur. Thus, b_2 versus t for various combinations of values of the parameters τ, α, and F may be determined from a single curve of y versus x.

Third Thermal in Series

The theoretical development for the third thermal in a series parallels that of the second. The momentum conservation equation for the third thermal is

$$\frac{d}{dt}\left(\frac{4}{3}\pi b_3^3 w_3\right)=F+\underline{\frac{d}{dt}\left(\frac{4}{3}\pi b_3^3 w_2\right)}. \tag{19}$$

The new term in eq (19) (underlined) contains the vertical velocity, w_2, of the second thermal at time $t+\tau$ where τ is the delay between the second and third thermals. The value of w_2 is assumed to be equal to the wake velocity encountered by the third thermal. It should be noted that any possible momentum gain from the wake of the first thermal in the series is also included because w_2 was computed from eq (12) and (13).

The momentum eq (19) can be simplified by integration and by application of the boundary condition $b_3=0$ at $t=0$ to

$$b_3^3 w_3=\frac{3Ft}{4\pi}+b_3^3 w_2. \tag{20}$$

Further simplification can be made by substituting for w_2 from eq (12) and for w_3 from

$$w_3=\frac{1}{\alpha_3}\frac{db_3}{dt}, \tag{21}$$

which is obtained from the volume equation in the form of eq (7) but for the third thermal (i.e., all subscripts$=3$).

This changes eq (20) to the form

$$b_3^3 \frac{db_3}{dt} = \frac{3\alpha_3 Ft}{4\pi} + b_3^3 \frac{\alpha_3}{\alpha_2} \frac{db_2}{dt}. \tag{22}$$

Equation (22) is easily solved by numerical methods. Other characteristics of the third thermal may be determined from equations that have the same form as those employed for the second thermal.

Comparison of eq (22) with eq (13) shows that the generalized momentum equation for the nth thermal in a series must be

$$b_n^3 \frac{db_n}{dt} = \frac{3\alpha_n Ft}{4\pi} + b_n^3 \frac{\alpha_n}{\alpha_{n-1}} \frac{db_{n-1}}{dt}, \tag{23}$$

which, for any n, can be iterated stepwise from a previously solved form such as eq (13) for $n=2$. Thus, we can in principle determine numerically the growth properties for any given number of thermals in a series, but, practically speaking, we need not continue beyond the point at which an equilibrium condition is reached. Some insight into this can be obtained from the generalized momentum equation written in the form

$$\frac{4}{3}\pi b_n^3 w_n = Ft + \frac{4}{3}\pi b_n^3 w_{n-1}. \tag{24}$$

The last term gives the amount of momentum gained from the wake of the preceding thermal, which is not the same as its total momentum because it includes only that amount of its mass that falls within the volume of the nth thermal. This is much smaller at any time t than the volume of the $(n-1)$th thermal. By iterating eq (24) back to $n=2$, we see from eq (13) that there is a contribution to the wake velocity from w_1, which, by the time the nth thermal is released, is proportional to

$$[t+(n-1)\tau]^{-1/2}.$$

This shows that the contribution of earlier thermals to the wake velocity may become comparatively small after a few have evolved, and thus the system does approach an equilibrium condition.

The validity of our assumption that the wake velocity is the same as the cap velocity of the preceding thermal must become more suspect as the spacing between thermals increases. The other constraint is that τ must be sufficiently long that overtaking does not occur. Thus, we see that the range of τ over which so simple a theory may be applied is quite limited.

3. EXPERIMENTS AND DATA ANALYSIS

The experimental investigations of second and third thermals in series were conducted in a Plexiglas tank 183 cm deep and 75 cm in diameter.[3] The tank was filled with water to a depth of 158 cm.

To avoid the problem encountered by Wilkins et al. (1971*a*) of not being able to distinguish second thermals from first thermals, we devised a new technique of cloud injection in which a clear salt solution was used for all thermals preceding the one under observation. The blue-dyed cloud material consisted of 50 percent water and 50 percent Sheaffer's Scrip Writing Fluid (Washable Blue #432) made into a 6.6-percent salt solution. Both clouds had a density of 1.045 g·cm^{-3}. Sufficient quantities of both cloud materials were made to insure uniformity throughout all the experiments conducted.

The cloud elements were injected into the tank of water from the top by quickly inverting a small beaker of material into the water. The injections consisted of 15 cm^3 each. The time interval between injections in series was 20 s in all experiments. Data were recorded at 2-s intervals for 20 s with a Nikon F Photomic-T 35-mm camera equipped with motor drive and remote triggering. A 28-mm F3.5 wide-angle lens was used to increase the viewing area. The use of backlighting with fluorescent lamps diffused through white tracing paper eliminated unwanted reflections.

The data were extracted using photogrammetric methods that have been described by Wilkins et al. (1969). The two cloud features that can be measured quantitatively for comparison with theory are cloud volume and height of rise. The volume estimate was made by assuming axial symmetry and dividing the thermal image into disks 2 cm in height. The diameter of each disk was measured for the purpose of calculating its volume. The widest distance from edge to edge of the disk was considered to be the diameter, introducing a negligible error. A volume estimate was obtained by summing up the volumes of all disks within the outline of the cloud. The height, h, of the thermal was measured directly from each frame, as simply the distance from the point of injection to the top of the thermal.

The values of b and h at 2-s intervals were obtained for each run for the three types of thermals: solitary (10 runs), second (11 runs), and third (9 runs). Mean values of b and h at 2-s intervals for each type of thermal were calculated at each data point.

The theory was developed on the assumption that the thermal originates from an instantaneous point source of buoyancy. The point source cannot be produced experimentally because it has as one of its boundary conditions $b=0$ when $t=0$. The experimental data were, therefore, subjected to a small virtual origin correction to make a satisfactory comparison with theory. A straight line was fitted to plotted values of h^2 versus t, using the method of least squares. The point at which the straight line intercepted the t axis ($h^2=0$) defined the location of the virtual origin, which was then translated to the intercept point to satisfy the boundary condition $h^2=0$ when $t=0$. The amount of translation was the time correction (about 1.5 s) to be applied to the data.

The entrainment rate, E, was calculated using the finite-difference form

$$E = \frac{1}{V}\frac{\Delta V}{\Delta t}$$

where ΔV is the incremental change of volume in an

[3] Mention of a commercial product does not constitute an endorsement.

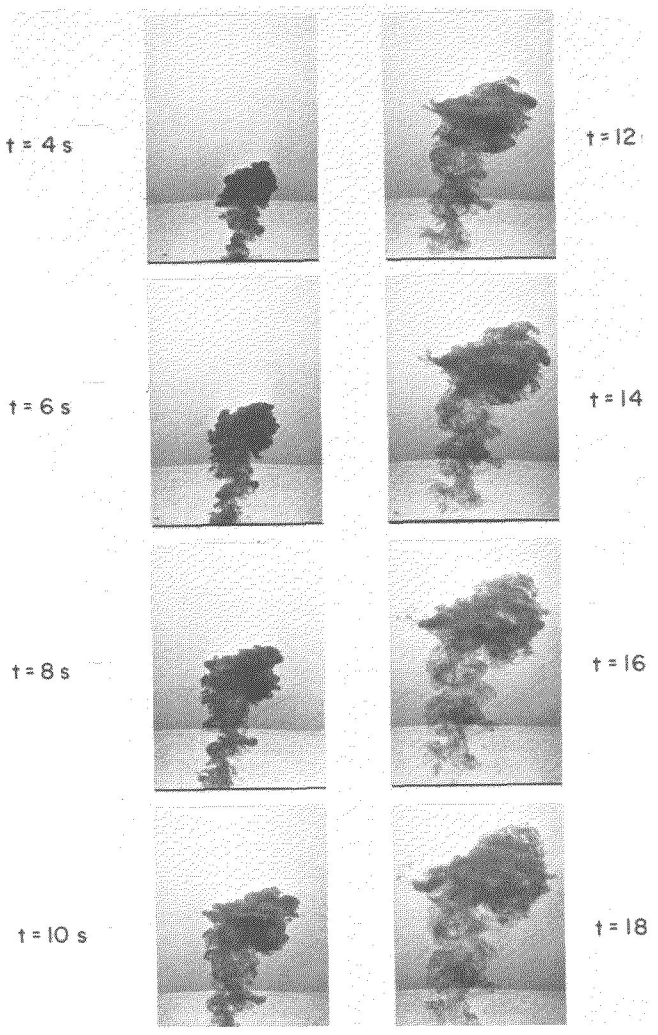

FIGURE 1.—Sequential photographs of a second thermal in a series, the preceding one being transparent. Time delay between thermals is 20 s.

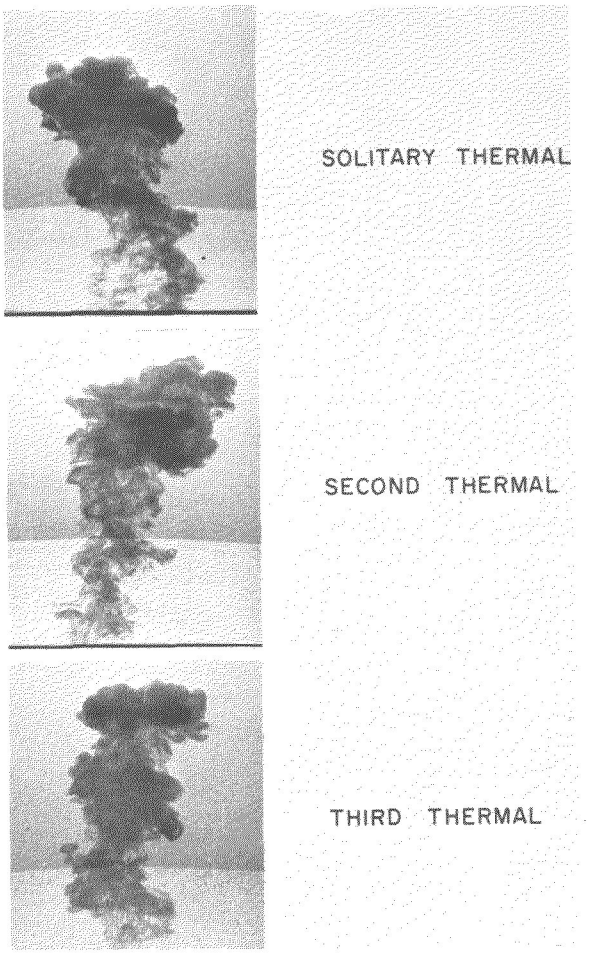

FIGURE 2.—Photographs of the three types of thermals at data time $t = 10$ s.

increment of time Δt. Values of V and ΔV were taken from smoothed mean value curves of volume versus time.

Ninety-five-percent confidence limits for the population mean were computed using the sample means and assuming a t-distribution. The confidence limits provide bounds to the estimate of the population mean. In this case, we can be 95-percent certain that the true mean of the population will lie between the limits shown. The limits were plotted to give some idea of the reliability of the mean values for comparison with theory.

4. COMPARISON OF LABORATORY SIMULATION WITH THEORY

The algorithm used in solving the theoretical equations for the second and third thermals in series was a fourth-order Runge-Kutta method using Gill coefficients (Ralston and Wilf 1960). The starting point used in this method was selected by the method shown in the appendix. The method does not permit starting with $t=0$ because the method depends on an evaluation of the first derivative, and, at this point, it is undefined. The starting point is important because, if it is anomalous, the whole curve will be erroneous.

A value of the entrainment constant, α, was determined for each type of thermal using the experimental values of sphere-equivalent radius and height. The values of α found were 0.244, 0.220, and 0.217 for the solitary, second, and third thermals, respectively. These values are consistent with values found by other investigators: 0.25 (Scorer 1957), 0.20–0.25 (Turner 1963), and 0.20 (Wilkins et al. 1969). Values of α determined experimentally are usually in the range of 0.20–0.25. The theoretical calculations for the various types of thermals were carried out using the value of α that was determined experimentally for that type, as this seems to provide the best test of the theory.

The sequential photographs in figure 1 show the second thermal in a series as seen in the experiments. This figure illustrates the unobstructed view of the second thermal when the transparent cloud material is used for the preceding thermal. It should be noted also that the second thermal is very similar in appearance to a solitary thermal, as seen by comparison with figure 2, and that it

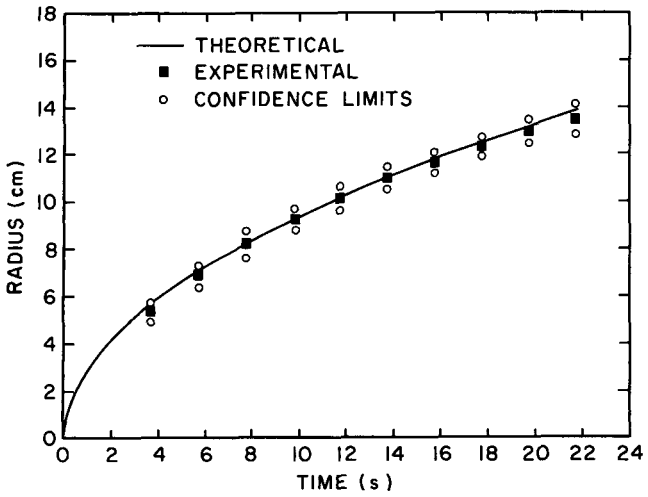

FIGURE 3.—Theoretical curve of sphere-equivalent radius vs. time for a solitary thermal compared with mean values of experimental data.

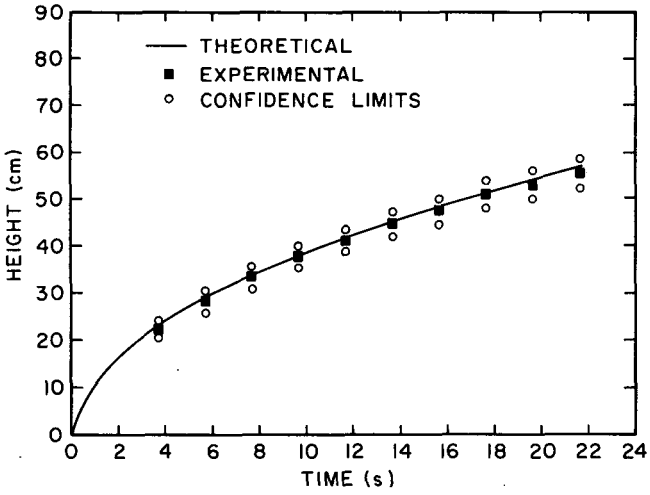

FIGURE 4.—Theoretical curve of height vs. time for a solitary thermal compared with mean values of experimental data.

would be difficult to detect the difference without a side-by-side comparison. Sequential photographs of the third thermal in series with two preceding transparent thermals also resemble photographs of the second thermal in series. For comparison, photographs of the three types of thermals at $t=10$ s are shown in figure 2. The solitary thermal can be easily distinguished from the second and third thermals because of the latters' enhanced height of rise. The second and third thermals are less easily distinguished from each other. The third thermal, however, does appear to have a much more prominent toroidal vortex.

Figures 3–6 show that the theoretical and experimental results agree very well for a solitary thermal and for the second thermal in series.

Figure 7 gives the numerical solution for the nondimensional form of the conservation equations of the second thermal. This curve may be used to evaluate sphere-equivalent radius and height of a second thermal at any time, t, and for any time delay, τ. The buoyancy force may also be varied, provided that the buoyancy forces of the first and second thermals are the same. This solution probably is not valid after overtaking occurs.

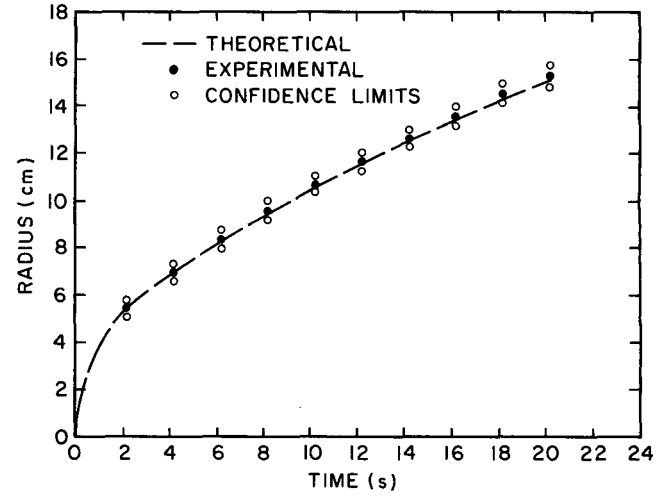

FIGURE 5.—Theoretical curve of sphere-equivalent radius vs. time for a second thermal in series compared with mean values of experimental data.

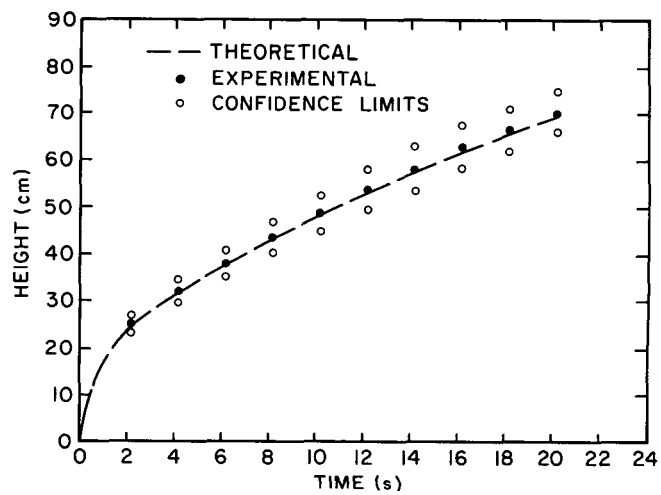

FIGURE 6.—Theoretical curve of height vs. time for a second thermal in series compared with mean values of experimental data.

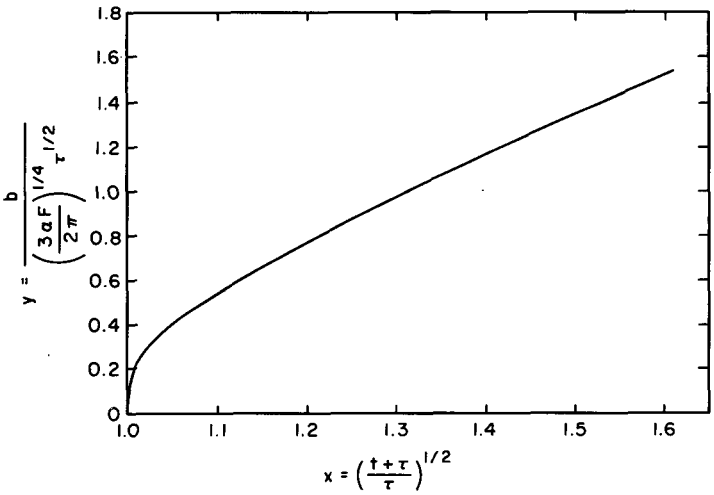

FIGURE 7.—Theoretical curve in nondimensional form for sphere-equivalent radius vs. time for the second thermal.

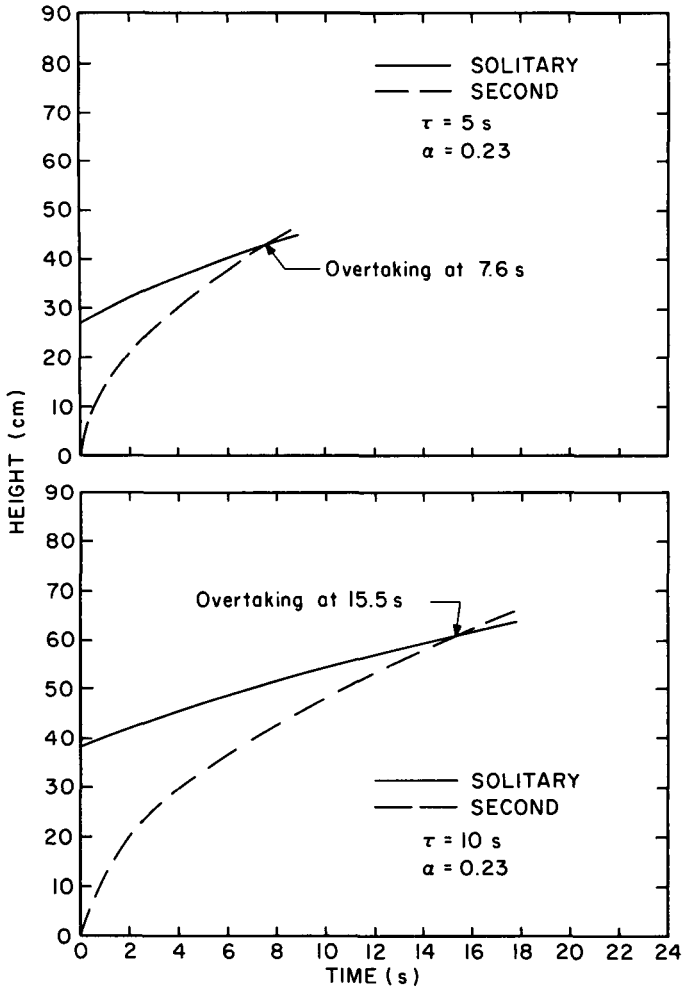

FIGURE 8.—Point of overtaking determined for thermals with 5 and 10 s delays by using the nondimensional curve of the second thermal.

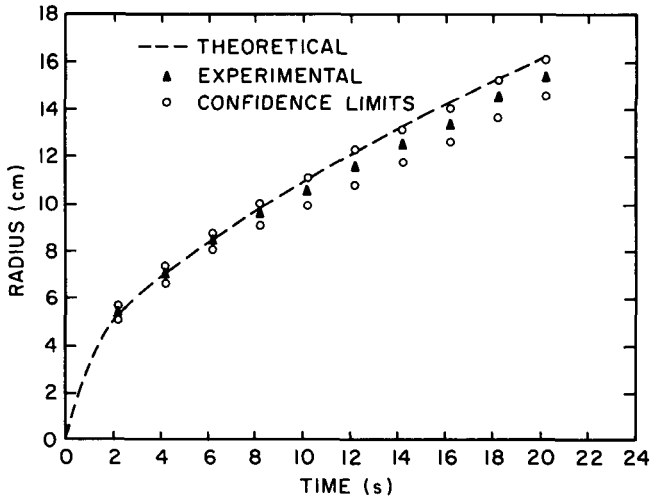

FIGURE 9.—Theoretical curve of sphere-equivalent radius vs. time for a third thermal in series compared with mean values of experimental data.

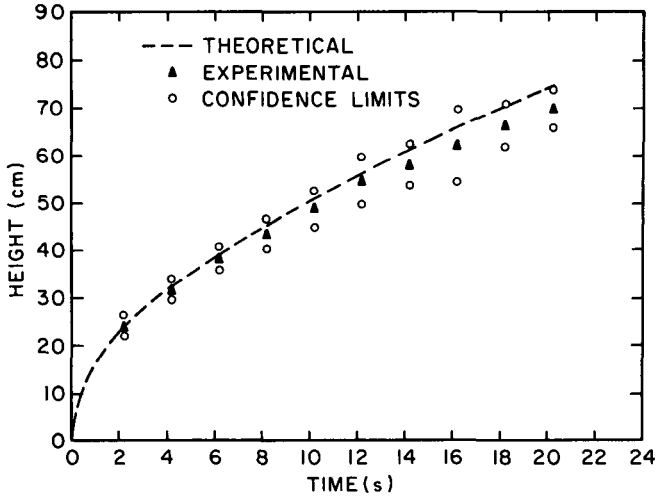

FIGURE 10.—Theoretical curve of height vs. time for a third thermal in series compared with mean values of experimental data.

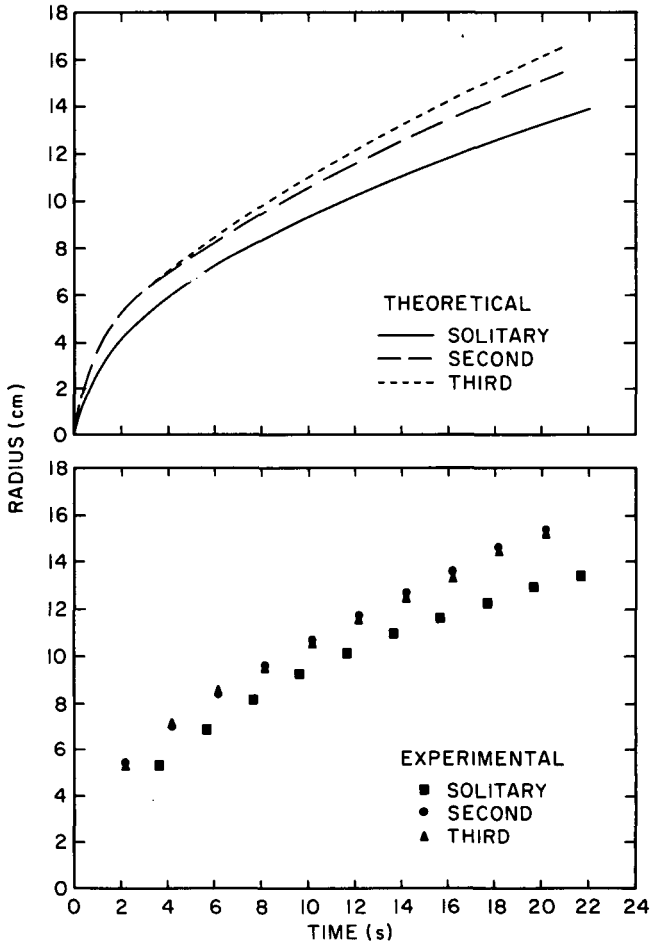

FIGURE 11.—Theoretical curves of sphere-equivalent radius vs. time and experimental mean values for the solitary, second, and third thermals.

The approximate point of overtaking is easily determined by plotting the height versus time curves of the solitary and second thermals. The nondimensional curve is used to determine values for the second thermal for any particular time delay, τ, and the solitary thermal is put into proper time frame by the value of τ selected. The intersection of the two curves will show the time at which overtaking occurs. The point of overtaking for time delays of 5 and 10 s are shown in figure 8 for thermals of the same buoyancy as those used in this investigation. It is

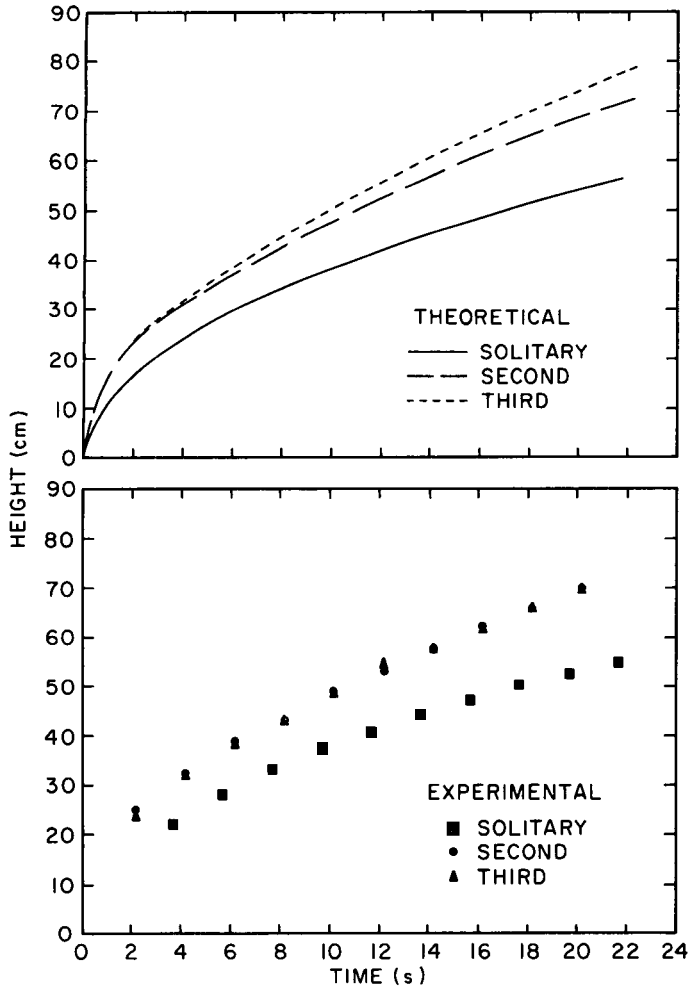

FIGURE 12.—Theoretical curves of height vs. time and experimental mean values for the solitary, second, and third thermals.

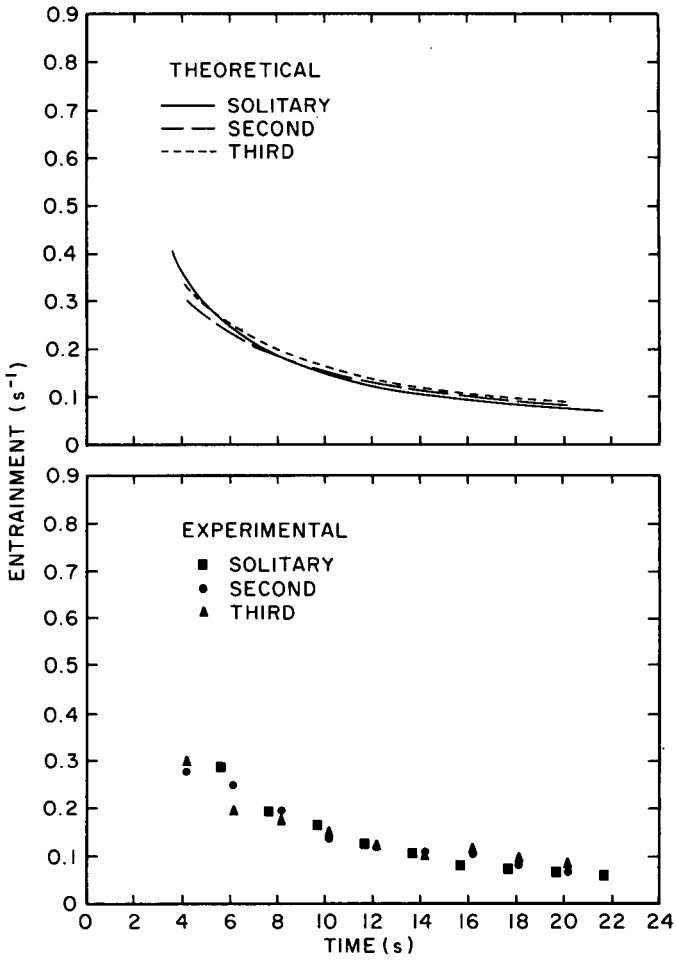

FIGURE 13.—Theoretical curves and experimental values of entrainment vs. time.

interesting to note that the time required for overtaking to occur in the case of a 10-s delay is about twice as long as for the 5-s delay, suggesting a possible linear relationship.

Figures 9 and 10 compare experimental data with theoretical values of sphere-equivalent radius and height of rise of a third thermal. The theoretical values of sphere-equivalent radius and height do not agree especially well with the experimental values after about $t=6$ s. It is obvious that the growth of the third thermal is slightly less than the theory would predict.

Figures 11 and 12 show the sphere-equivalent radius curves and height curves for the three types of thermals simultaneously. These show enhancement in the growth of both the second and third thermals relative to that of the solitary thermal. The enhancement of the third thermal over the second thermal is not predicted to be as great as the enhancement of the second thermal over the solitary one. From the experimental data, we find that there is no significant difference between the second and third thermals. This is at least in the right direction to agree with theory, although the fit is less than perfect.

Figure 13 shows the theoretical curves and experimental values of entrainment versus time. The theoretical curves are all grouped very closely and show very little difference for the three types of thermals. The same is true for the experimental data points, and the agreement is also good for the magnitudes of the entrainment rates.

5. CONCLUSIONS

The main contributions from the research reported here lie in the improvements in cloud simulation technique and in the theory for successive thermals. The new technique has provided more accurate measurements of cloud growth and has avoided the obscuration of successive clouds due to merging. As more accurate measurements became available, it became obvious that the earlier theory (Wilkins et al. 1971*a*) for wake effects needed to be changed, and this was accomplished.

The theoretical development for second and third thermals in a series predicts that successive enhancement of growth rate will occur due to momentum gains from the wakes of preceding thermals. The theory developed for the second and third thermals was based on conservation of total momentum to account for the enhancements.

The close agreement of the theoretical and experimental results for the solitary thermal reaffirms the theory of Morton et al. (1956). The importance of this agreement to

the present analysis is that our predictions for successive thermals are based on an extension of that theory.

Experimental results of the second thermal do show, correctly, the amount of enhancement of the growth rate of the second thermal over that of the solitary thermal. This agreement tends to verify the theory regarding wake effects on a second thermal. The nondimensional solution of the momentum equation provides a description of the second thermal for various values of cloud buoyancy and time delay, and the curve can be used with the height versus time curve of the solitary thermal to predict when overtaking will occur for various time delays.

The theoretical and experimental values for the third thermal do not agree especially well after about $t=6$ s. The experimental values for the second and third thermals show that there is no significant difference between them. This indicates that the third thermal is encountering a wake similar to that encountered by the second thermal. It may be that an equilibrium condition is reached with only a very few thermals in a series. Another possible explanation is that, while the theory for the third thermal includes momentum gain from the wake of the first thermal, experimentally, the wake was too dissipated (possibly due to viscosity) to be detected. During the observation of the third thermal, the age of the first thermal increases from 40 to 60 s. It is possible that tank wall effects may be present by this time, although the solitary thermal is not observed to contact the bottom of the tank within 60 s.

The results of this investigation suggest other experimental variations that might be made to improve further the understanding of successive thermals. It would be of interest to learn whether or not the theory for the third thermal would be validated by a statistically more significant set of experimental data. Variation of the time delay between injections is of interest to test the validity of the theory for shorter time delays. An attempt should be made also to derive a theory describing the overtaking of thermals and to test the theory by simulation experiments. Finally, the new theory and laboratory simulations should be extended to the more complex case of successive thermal interactions in a rotating environment.

APPENDIX: METHOD OF CHOOSING AN INITIAL VALUE FOR THE COMPUTATIONAL SCHEME

The initial value for the Runge-Kutta method is estimated from a solution that is an approximation to the true curve. We begin by letting $\xi=x-1$ in eq (16) to displace the curve to the origin. The new equation becomes

$$y^3(y'-1)=\xi(\xi^2+3\xi+2) \tag{25}$$

where the prime now denotes a derivative with respect to ξ. A trial solution of the form $y=A\xi^m$ gives

$$A^3\xi^{3m}(mA\xi^{m-1}-1)=\xi(\xi^2+3\xi+2), \tag{26}$$

which has the proper form as $\xi\to 0$ only if $m=1/2$. We then have

$$\frac{1}{2}A^4-A^3\xi^{1/2}=\xi^2+3\xi+2 \tag{27}$$

and note that, very near the origin (very small ξ), we can evaluate the coefficient A as $A^4=4$. Thus, the required approximate solution is $y^2=2\xi$, and the only question that remains is how near the origin we must choose ξ_1 to compute an acceptably accurate curve. We satisfied this requirement by computing the curve from ξ_1, y_1 sufficiently near the origin that a trial computation using a starting value of ξ one-tenth as large as ξ_1 would make a difference of no more than 2 percent at the farthest point on our curve.

ACKNOWLEDGMENTS

The authors express their gratitude to Rex L. Inman and Claude E. Duchon for suggestions and for critical review of the manuscript. We thank Wallace H. Chaplin, U.S. Air Force, for assistance with the simulation experiments. This research was supported by the Atmospheric Sciences Section, National Science Foundation, under grants Nos. GA-16350 and GA-27665.

REFERENCES

Batchelor, G. K., "Heat Convection and Buoyancy Effects in Fluids," *Quarterly Journal of the Royal Meteorological Society*. Vol. 80, No. 344, London, England, July **1954**, pp. 339–358.

Morton, B. R., Taylor, Geoffrey I., and Turner, J. S., "Turbulent Gravitational Convection From Maintained and Instantaneous Sources," *Proceedings of the Royal Society of London*, Ser. A, Vol. 234, No. 1196, England, Jan. 24, **1956**, pp. 1–23.

Ralston, A., and Wilf, H. S., *Mathematical Methods for Digital Computers*, John Wiley & Sons, Inc., New York, N.Y., **1960**, 387 pp. (see pp. 110–120).

Sasaki, Yoshikazu, "Some Dynamical Aspects of Atmospheric Convection," *Tellus*, Vol. 19, No. 1, Stockholm, Sweden, **1967**, pp. 45–53.

Schauss, Roger H., "Numerical and Laboratory Simulations for the Investigation of Wake Effects on Successive Thermals," M. S. thesis, University of Oklahoma, Norman, **1970**, 65 pp.

Scorer, Robert S., "Experiments on Convection of Isolated Masses of Buoyant Fluid," *Journal of Fluid Mechanics*, Vol. 2, Pt. 6, Taylor & Francis, Ltd., London, England, Aug. **1957**, pp. 583–594.

Turner, J. S., "Model Experiments Relating to Thermals with Increasing Buoyancy," *Quarterly Journal of the Royal Meteorological Society*, Vol. 89, No. 379, London, England, Jan. **1963**, pp. 62–74.

Wilkins, Eugene M., Sasaki, Yoshikazu, Friday, Elbert W., Jr., McCarthy, John, and McIntyre, James R., "Properties of Simulated Thermals in a Rotating Fluid," *Journal of Geophysical Research, Oceans and Atmospheres*, Vol. 74, No. 18, Aug. 20, **1969**, pp. 4472–4486.

Wilkins, Eugene M., Sasaki, Yoshikazu, and Schauss, Roger H., "Interactions Between the Velocity Fields of Successive Thermals," *Monthly Weather Review*, Vol. 99, No. 3, Mar. **1971***a*, pp. 215–226.

Wilkins, Eugene M., Sasaki, Yoshikazu, and Schauss, Roger H., "Vortex Formation by Successive Thermals: A Numerical Simulation," *Monthly Weather Review*, Vol. 99, No. 7, July **1971***b*, pp. 577–592.

Woodward, Betsy, "The Motion in and Around Isolated Thermals," *Quarterly Journal of the Royal Meteorological Society*, Vol. 85, No. 364, London, England, Apr. **1959**, pp. 141–151.

[*Received August 2, 1971; revised February 22, 1972*]

UDC 551.551.5:551.557.5:551.576.1:551.507.362.2(084.1)"1970.12.28/29"

PICTURE OF THE MONTH
A Turbulent Region

ARTHUR H. SMITH, JR.—*Environmental Technical Applications Center, U.S. Air Force, Washington, D.C.*

Satellite photographs of certain atmospheric conditions can frequently be used in locating specific regions of high risk of turbulence occurence (high risk areas). In particular, the cloud patterns associated with polar and subtropical jet streams, which are known as areas of high turbulence probability, are distinguishable on satellite photographs. These high risk areas are easily verified when they occur over data-rich areas and, if similar cloud patterns are identified over little-traveled, data-sparse regions, the identification and forecasting of turbulence can most certainly be improved.

One such example of cloud patterns associated with a high risk area occurred on Dec. 28–29, 1970. The jet stream cloud patterns associated with the turbulent areas can be seen in figure 1. The clouds associated with the subtropical jet stream originate in the intertropical convergence zone (A) and sweep northeastward in an anticyclonically curved arc (B,C). According to Anderson (1969), the polar jet stream can be located where there is a change from unstable clouds to stable clouds (D,E). While it becomes difficult to pinpoint an exact location of the polar jet stream as it continues eastward (F,G,H), careful examination does reveal a slight shadowline (F to G) from the jet stream cirrus appearing on the lower clouds. Mountain-wave clouds associated with both the polar jet stream (I) and the subtropical jet stream (J), plus the

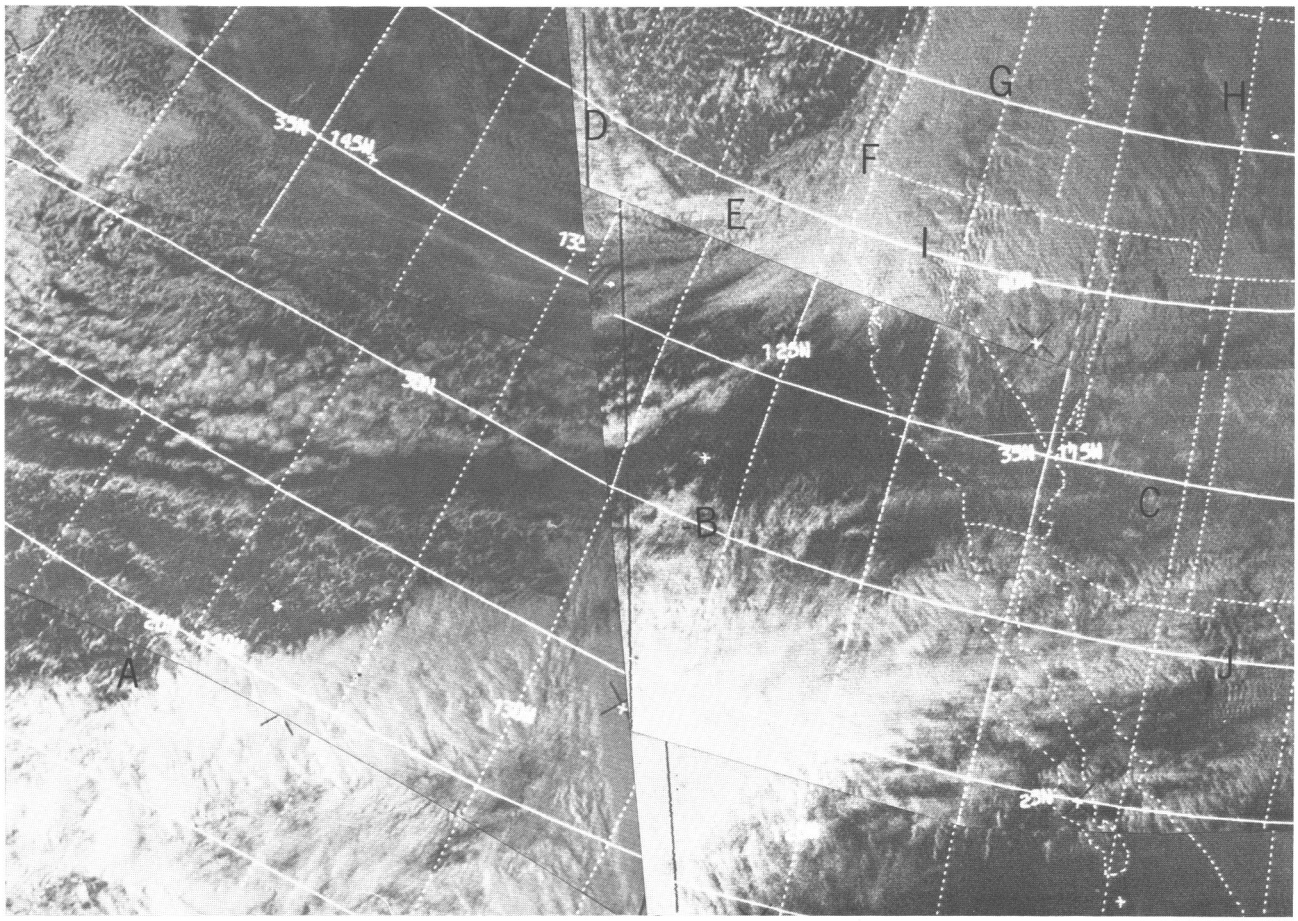

FIGURE 1.—ITOS (improved TIROS operational satellite) 1 view, pass 4246 at 2230 GMT, Dec. 28, 1970, and pass 4247 at 0000 GMT, Dec. 29, 1970.

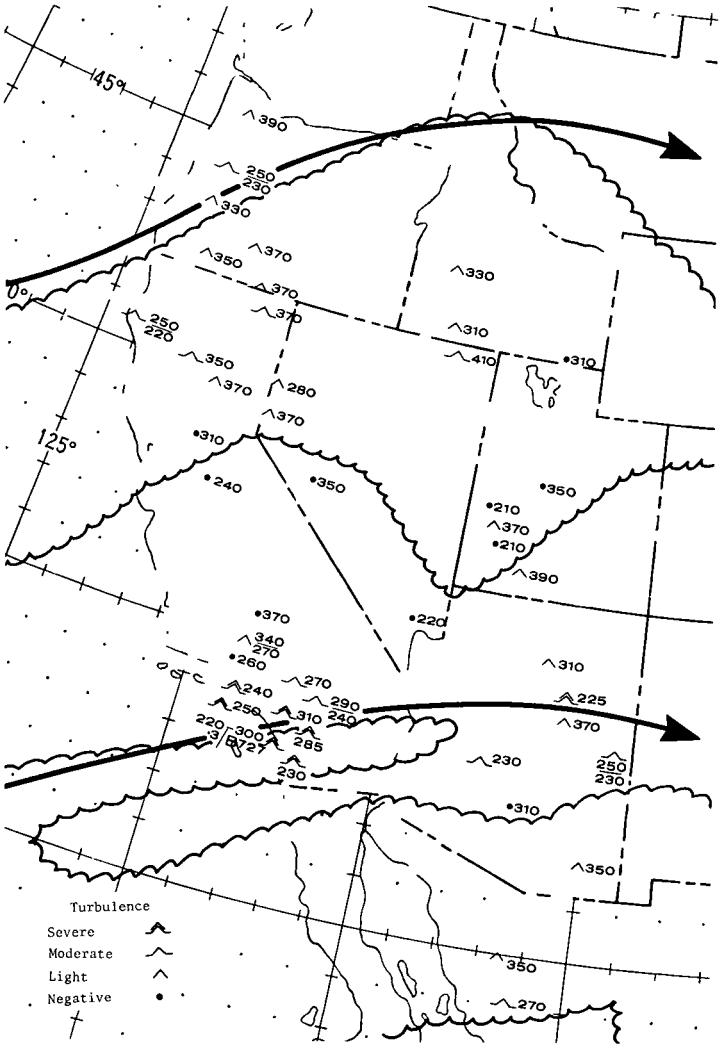

FIGURE 2.—Turbulence reports for the period 0000–0600 GMT, Dec. 29, 1970. Height is in hundreds of feet. Jet streams are shown as solid arrows. Areas of cirrus (taken from fig. 1) are enclosed by scalloping.

area of transverse bands within the subtropical jet cloud pattern, are other areas indicative of a high risk of turbulence observable on meteorological satellite pictures.

These two jet streams tend to converge in a manner similar to that described by Kadlec (1966) with the northern (polar) jet stream in a trough-ridge pattern and the subtropical (southern) jet in a broad anticyclonically curved pattern. In general, it has been noted that, if the jets converge to within 400 mi or less, a cirrus sheet associated with both jets is continuous from the upper trough to the next downstream ridge associated with the polar jet. It is in and near portions of this cirrus sheet that regions of moderate or greater clear air turbulence (CAT) are encountered. In this particular case, the two jets converge to within about 750 mi and the cirrus sheet is not continuous between the two jets. Figure 2 shows that most of the actual turbulence is in or near the cirrus, not in the clear air between the two jets.

The distribution of turbulence both in the horizontal and vertical compares favorably with the "type B"

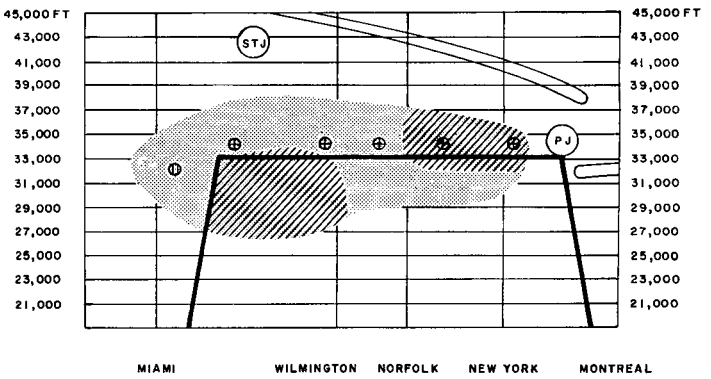

FIGURE 3.—Vertical cross-section of polar and subtropical jet streams, cirrus pattern, and associated turbulence areas for model type B (Kadlec 1966). PJ is the polar jet core, STJ is the subtropical jet core, the stippled area represents polar and subtropical jet stream cirrus, and the crosshatched area indicates moderate or greater turbulence.

turbulence model by Kadlec (1966) depicted in figure 3. In the horizontal, there is a concentration of moderate and severe turbulence reports, associated with the subtropical jet stream in the dense-traffic area near Los Angeles, Calif., and a lesser number of reports further north and east as traffic density decreases. North of the subtropical jet over central California, Nevada, and Utah, the air is relatively smooth with negative and light turbulence reports prevailing. A secondary maximum of moderate turbulence appears over northern California, southern Oregon, and extreme northern Nevada in association with the polar jet and the mountain-wave clouds (I in fig. 1).

In the model, turbulence associated with the polar jet is at a higher altitude (32,000–37,000 ft mean sea level) than that with the subtropical jet (26,000–33,000 ft). The present example has a similar vertical structure. The turbulence with the polar jet stream is generally above 30,000 ft while, with the subtropical jet stream, the moderate to severe turbulence is concentrated below 30,000 ft.

The north–south vertical cross-section (fig. 4) shows a pattern similar to figure 3 with the subtropical jet at a higher altitude than the polar jet. An area of coincident, strong, horizontal and vertical wind shear is a favored region for moderate to severe turbulence (George 1960). The area from San Diego, Calif., to just south of Vandenberg Air Force Base, Calif., between 21,000 and 26,000 ft is such an area and was characterized by a large number of severe turbulence reports. The horizontal and vertical wind shear with the polar jet stream at this time is not as strong as with the subtropical jet. Also, in the polar jet area, the shear has a much greater vertical extent, from near 25,000 to over 35,000 ft. The turbulence associated with this weaker shear is reported as light to moderate and has a large vertical extent with a slight concentration between about 33,000 and 37,000 ft above mean sea level over the jet core. Wind speeds are low and shear is small from north of Vandenberg Air Force Base to northern California. No turbulence is reported in that area.

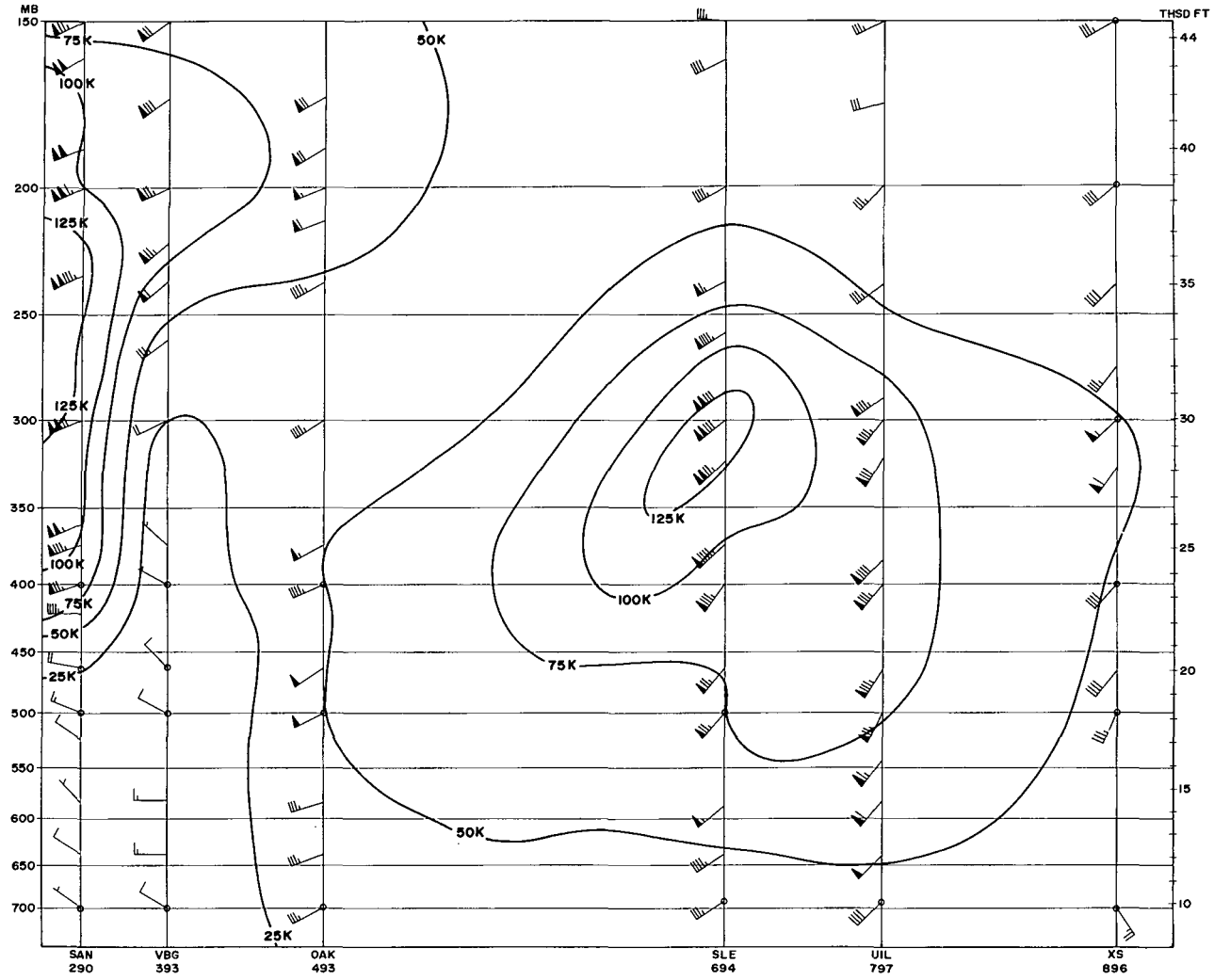

FIGURE 4.—A north–south vertical cross-section for 0000 GMT, Dec. 29, 1970.

REFERENCES

Anderson, Ralph K., et al., "Application of Meteorological Satellite Data in Analysis and Forecasting," *AWS Technical Report* 212, U.S. Air Weather Service, Washington, D.C., June **1969**, sections separately paged.

George, J. J., *A Method for the Prediction of Clear Air Turbulence*, Eastern Air Lines, Atlanta, Ga., Aug. **1960**, 17 pp.

Kadlec, Paul, "Flight Observations of Atmospheric Turbulence," *Final Report*, Contract No. FA66WA–1449, Federal Aviation Agency, Washington, D.C., **1966**, 52 pp.